# Fluctuations of High Clouds and 500-mb Geopotential Heights in Baroclinic Waveguides

THOMAS P. CHARLOCK

*Atmospheric Sciences Division, NASA Langley Research Center, Hampton, Virginia*

FRED G. ROSE

*Lockheed Engineering and Sciences Company, Hampton, Virginia*

(Manuscript received 5 March 1990, in final form 30 July 1990)

ABSTRACT

A time filter that passes waves with periods in the 2.5–6.0 day band is applied to a six-winter record of the Nimbus-7 THIR/TOMS high cloudiness and the NMC 500-mb geopotential height in the northern extratropics. The strongest correlations between fluctuations in geopotential and high cloudiness are found in the baroclinic waveguides, where the fields of both geopotential and high cloudiness exhibit large variabilities. Over many grid points in the waveguides, positive anomalies in high cloud areas are found to be approximately one-third of a wavelength to the east of negative anomalies in 500-mb heights (band-pass troughs), and negative anomalies in high cloud areas are found to be approximately one-sixth of a wavelength to the west. A map of the standardized anomalies in the cloud area associated with height fluctuations above the mean forms a simple negative of the map of the cloud anomalies associated with height fluctuations below the mean. The analysis presented here suggests that the high cloud structures of baroclinic waves are less spatially coherent than the internal geopotential height structures. Over the North Pacific, small-scale (latitudinal wavenumber 13–18) fluctuations in geopotential appear to play a greater role in forcing high cloudiness than do medium-scale (latitudinal wavenumber 7–12) fluctuations in geopotential.

## 1. Introduction

The task of observing and simulating global cloud fields presents a formidable challenge to the remote sensing and modeling communities. Fluctuations in cloudiness, which are often associated with small perturbations in vertical velocity, provide a graphic illustration of variations in the general circulation of the atmosphere. Some of the most seminal studies of atmospheric circulation (i.e., Kuo 1953) have emphasized relationships between the vertical velocity, temperature, and geopotential height fields. Some of these relationships can be investigated with newly available satellite data.

Studies of cloudiness (Cahalan et al. 1982) and geopotential height (Blackmon 1976) have shown that in the extratropics, fluctuations in large-scale cloudiness occur more rapidly and on smaller spatial scales than do fluctuations in the geopotential height (Gutzler and Mo 1983). Cahalan et al. (1982) used outgoing longwave radiation (OLR) from twice-daily satellite observations as a surrogate for large-scale cloudiness. In dynamically active regions of the midlatitudes, the autocorrelation of OLR was found to vanish within 2–3 days, and within 12 hours for 2.5° × 2.5° grid boxes in an Eulerian frame. This is in contrast to the geopotential height analysis of Blackmon (1976), which found that most of the temporal variability of the 500-mb heights was captured by a low-pass filter that culled fluctuations with periods greater than 10 days. Blackmon et al. (1977) associated most of the transient synoptic-scale disturbances with geopotential fluctuations captured by a band-pass filter in the 2.5–6.0 day scale. The regions associated with high geopotential variability in the approximate band-pass (2.5–6.0 day) time scale have been dubbed "storm tracks," although more recently the term "baroclinic waveguide" has been suggested (Wallace et al. 1988; hereafter denoted WLB).

Radiation and cloudiness also have substantial variability in the band-pass time scale. Charlock et al. (1989) used a general circulation model (GCM), satellite and National Meteorological Center (NMC) data to investigate the band-pass cross correlation between OLR (again as a cloud surrogate) and the poleward component of the horizontal wind. In rough agreement with quasi-geostrophic theory, OLR and the poleward component of the horizontal wind were found to be negatively correlated. Clouds tend to form at the leading edge of a trough, where the wind has a positive poleward component and a positive vertical component. These clouds depress the OLR. The local band-

*Corresponding author address:* Dr. Thomas P. Charlock, Atmospheric Sciences Division, Mail Stop 420, NASA Langley Research Center, Hampton, VA 23665-5225.

pass correlation of OLR and the poleward component of the wind was found to be the strongest in the vicinity of the midlatitude baroclinic waveguides.

Here the spatial phase relationship between band-pass fluctuations in cloudiness and the atmospheric circulation are investigated with explicit satellite retrievals of high cloud areas (Stowe et al. 1988, 1989) and the NMC 500-mb geopotential heights. Concepts developed in WLB, Blackmon et al. (1984a,b), and Cahalan et al. (1982) are followed. The Stowe et al. (1988, 1989) satellite cloud retrievals permit investigation of the relationship of fluctuations in geopotential height and cloudiness at approximately the same vertical levels. Here the spatial correlation of a base grid point in the height field with the full field of the height is used to define the structure of a climatological band-pass geopotential wavetrain; the spatial correlation of the same base grid point in the height field with the full field of cloudiness then displays the phase relationship of the fluctuations in cloudiness to the fluctuations in geopotential. Charlock et al. (1989) did not employ explicit satellite cloud retrievals or use spatial correlations to diagnose phase relationships in detail.

The structure of the remainder of this paper is as follows. Section 2 describes the data. An overview of the mean and band-pass-filtered high cloud and geopotential height fields is given in section 3. Sections 4 and 5 employ band-pass filtered data exclusively. In section 4, the spatial correlation of a base grid point in 500-mb height is developed with the full fields of both height and cloudiness. Section 4 also displays composites of the high-cloud field that are associated with respectively positive and negative fluctuations in geopotential height. A full depiction of the spatial correlation of geopotential and high cloudiness poleward of 20°N is given in section 5. A discussion is found in section 6.

## 2. Data

NMC analyses have been reviewed by Trenberth and Olson (1988). An NMC 500-mb geopotential height time series from the National Center for Atmospheric Research (NCAR) was used. The data are in a 5° × 5° grid. Missing data points were filled with adjacent values.

The high-cloud data used to generate the figures in this work were based on Nimbus-7 retrievals. Ancillary calculations were based on high-cloud retrievals from the International Satellite Cloud Climatology Project (ISCCP). The use of Nimbus-7 and ISCCP high-cloud retrievals is regarded as an advance over the use of OLR values as a simple surrogate for high clouds. The OLR signal is strongly influenced by surface temperature, humidity, and clouds at various levels.

Stowe et al. (1988, 1989) employed threshold techniques to identify the low-, middle-, and high-cloud areas using Nimbus-7 Temperature Humidity Infrared Radiometer (THIR) 11.5-$\mu$m radiances and Total Ozone Mapping Spectrometer (TOMS) ultraviolet radiances, U.S. Air Force surface temperature data, and climatological vertical temperature lapse rates. The high-cloud retrievals are considered to be the most accurate because the middle and low clouds can be obscured to the spacecraft's view. The Nimbus-7 clouds are classified as high (rather than middle) level based on a scale that is latitude-dependent. Clouds with tops greater than 7 km (above mean sea level) equatorward of 30° latitude are high. Poleward of 30°, a high-cloud threshold is defined to vary with the cosine of the latitude; the threshold falls to 4 km at the pole. In midlatitudes during Northern Hemisphere (NH) winter, the 500-mb surface is commonly found at a height of 5500 gpm, approximately the same level as the Nimbus-7 high clouds.

The cloud retrievals were obtained from the Nimbus-7 CMATRIX tapes in spatial bins with an area equivalent to 4.5° × 4.5° at the equator. The Nimbus-7 equator crossing times are approximately local noon and midnight, permitting retrievals twice per day over most of the globe. Some geographical points were observed by the satellite more frequently than twice per day; in such cases, the CMATRIX tapes contain the observation closest to the satellite. We placed the ascending and descending node Nimbus-7 retrievals in a record corresponding to the closest 0000 UTC or 1200 UTC rawinsonde observing time and spatially interpolated the 5° × 5° NMC data into the CMATRIX grid. There can be a difference of up to 6 hours in the satellite and rawinsonde observing times; the data are generally asynoptic. Charlock et al. (1989) addressed the problem of the asynopticity of polar orbiter satellite data and rawinsonde observations by using the 31-point band-pass filter of Blackmon (1976), which passes waves with periods between 2.5 and 6.0 days. The same approach has been used here.

The analysis covers NH winter, here defined as December–February. The Nimbus-7 cloud record begins in April 1979 and ends in March 1985. Six winters of Nimbus-7 and NMC data, beginning with December 1979 and ending with February 1985, are covered here. Comparison of the 500-mb statistics with those of Blackmon et al. (1984a,b), who used longer records, indicated that six winters provide a sufficient length of record for generally stable band-pass statistics.

Part of the analysis in section 4 was repeated with early ISCCP data (Schiffer and Rossow 1985; Rossow et al. 1988), which were available for a single winter (December 1983–February 1984). ISCCP data provide cloud retrievals in 280 km × 280 km equivalent area grid boxes every 3 h. ISCCP data were used as a check on the present approach to the asynopticity problem: a comparison of band-pass geopotential–cloud correlations was made with ISCCP (3-h and sampled at the 0000 and 1200 UTC rawinsonde times) and the Nimbus-7 (twice-daily and usually different than the 0000

and 1200 UTC rawinsonde times) data. ISCCP data are based on a single polar orbiter and four geostationary satellites. While Nimbus-7 cloud data are specified in three vertical levels (low, middle, or high), ISCCP cloud data are specified in seven vertical pressure levels. When ISCCP data were used, high clouds were defined as those with tops at 440 mb or above.

## 3. Overview of fields

### *a. Display of 500-mb and high clouds*

The NH winter mean jet and trough positions can be determined by an examination of the mean 500-mb geopotential height for our 6-yr record (Fig. 1a). In computing the standard deviation of the band-pass-filtered approximation of the geopotential streamfunction (Fig. 1b), the heights were first multiplied by the factor $\sin 45°/\sin L$, where $L$ is latitude. WLB point out that this small latitudinal adjustment produces height statistics that are more directly comparable with statistics based on wind and vorticity. The structure of the standard deviation field in Fig. 1b is similar to that in Figs. 1a,b of WLB, where different filters (high-pass and 24-h difference) were employed. WLB found that their baroclinic waveguide results were not strongly filter-dependent, provided that waves with periods of a few days were retained. The band-pass filter that is used here is more appropriate for the task of correlating the satellite cloud retrieval and NMC data. The band-pass filter removes the highest frequencies, where the effects of the asynopticity of the satellite cloud retrieval and NMC data are most pronounced.

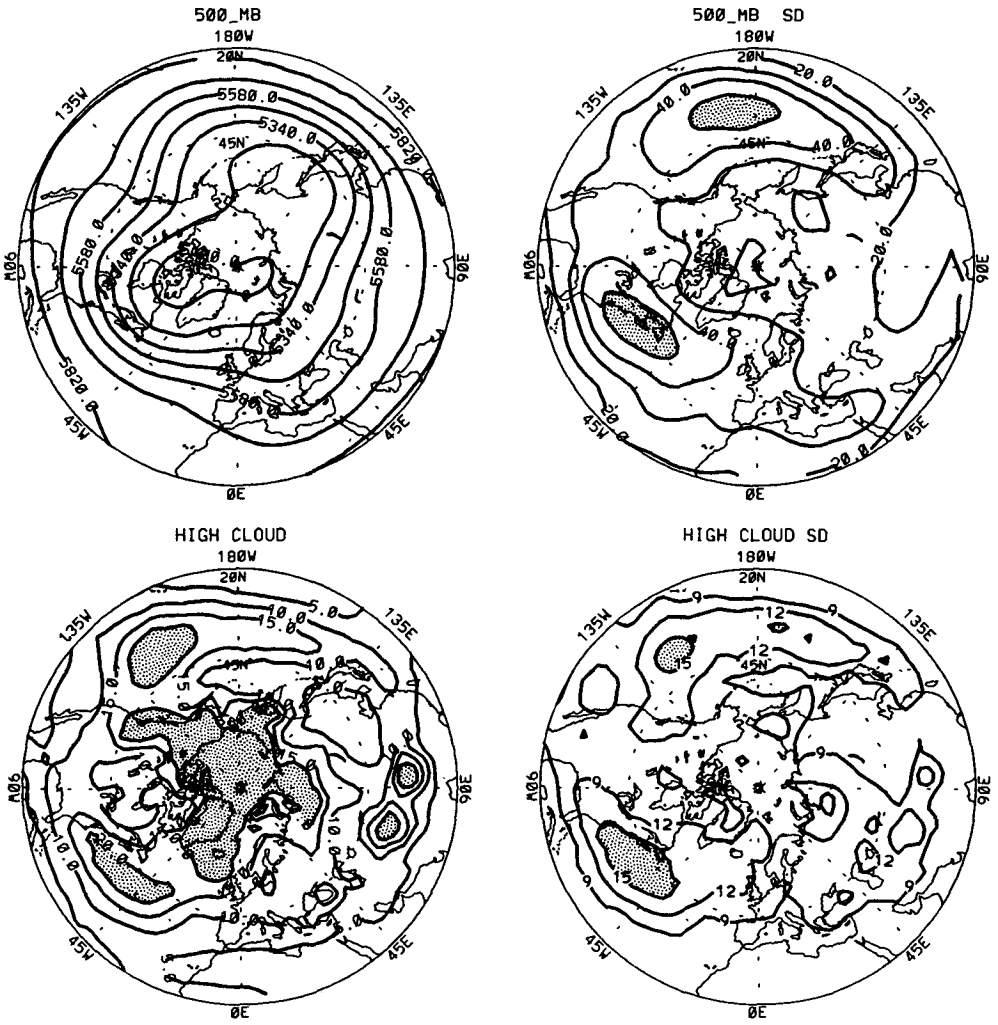


FIG. 1. (a) Upper left panel. The mean height of the 500-mb surface in gpm for the six-winter (December–February) record poleward of 20°N. (b) Upper right panel. The standard deviation of the band-pass-filtered approximation of the 500-mb geopotential streamfunction. (c) Lower left panel. The mean high cloud area in percent. The highest contour plotted is 20 percent. (d) Lower right panel. The standard deviation of the band-pass filtered high cloud area. The contour interval is 3 percent.

In plotting mean high-cloud fractional area (Fig. 1c), contours greater than 0.20 have been excluded. Quite large values of high-cloud area were retrieved poleward of 60°N. Temperature inversion and isothermal lapse rate conditions limit the applicability of infrared threshold cloud retrieval schemes. These conditions are frequently obtained poleward of 60°N during the winter. While results are displayed for all areas of the NH poleward of 20°N, most of the discussion focuses on the regions equatorward of 60°N.

### *b. Relationship of 500-mb and high clouds*

In the midlatitudes, maxima in the NH winter mean areal coverage of high clouds (Fig. 1c) are found over the central and eastern Pacific, northwestern North America, western and central Atlantic, and the Himalayas. The midlatitude oceanic maxima in seasonal mean high-cloud areas are displaced from the maxima in seasonal mean 500-mb vertical velocity reported in White (1983). Seasonal mean oceanic high cloud maxima are even found over seasonal mean 500-mb subsidence zones as inferred by vertical velocities computed with **Q** vector, vorticity balance, and adiabatic assumptions (see Figs. 8, 9, and 10 in White 1983, where at 40°N, 60°W subsidence is indicated in the region of our North Atlantic cloud maximum). This is found not to be surprising. The time-mean flow is more important in forcing the seasonal mean vertical motion than are the transient eddies (White 1983), and the clouds, which are mostly high-frequency phenomena, generally respond to the faster dynamical events. The midlatitude oceanic seasonal mean maxima in cloudiness (Fig. 1c) are located at or to the east of the maxima in the standard deviation of the band-pass geopotential streamfunction (Fig. 1b). A large standard deviation of the band-pass streamfunction indicates storm activity that can generate clouds.

The spatial phase relations between the fluctuations in the cloudiness and the streamfunction will be analyzed in detail in sections 4 and 5. Presently it is noted that the relative spatial relationships between the maxima in the band-pass-filtered streamfunction and the high cloudiness are somewhat different in the Atlantic and the Pacific. In the western North Atlantic at 55°W, the strongest mean (Fig. 1c) and band-pass-filtered (Fig. 1d) cloud features are displaced about 10° to the east of the corresponding maximum in the band-pass standard deviation in the streamfunction (Fig. 1b). In the central North Pacific, the strongest mean and band-pass-filtered cloud features are centered at 150°W, displaced about 25° to the east of the corresponding maximum in the band-pass-filtered standard deviation in the streamfunction at 175°W.

The more eastward displacement of the cloud features relative to the band-pass streamfunction maxima in the Pacific (25°) as opposed to the Atlantic (10°) appears to be a result of contrasts in the spatial scale of streamfunction fluctuations over the two ocean basins. Blackmon (1976) has described the spatial scale of the 500-mb height fluctuations; with slight latitudinal adjustments, they correspond to 500-mb streamfunction fluctuations. Band-pass 500-mb fluctuations in both the Atlantic and Pacific are dominated by small-scale (latitudinal wavenumber 13–18) and medium-scale (latitudinal wavenumber 7–12) waves (see Fig. 5 in Blackmon 1976). In the Atlantic, the maxima of the fluctuations in the small-scale and medium-scale 500-mb waves are approximately collocated. In the Pacific, however, the maxima of the fluctuations in the small-scale 500-mb waves (located at 160°W) and the medium-scale 500-mb waves (located at 180°W) are geographically separated. The proximity of the mean and band-pass high-cloud features in the Pacific to the maxima in the band-pass small-scale 500-mb waves at 160°W (Fig. 5d in Blackmon 1976) suggests that the small-scale 500-mb waves may have more impact on cloudiness.

The continental maxima in seasonal mean high cloudiness over northwestern North America and the Himalayas are collocated with, respectively, a ridge and a region of moderate zonal flow at 500 mb (Fig. 1a). Both continental high cloud maxima are approximately collocated with the mean seasonal upward vertical velocity zones of White (1983). Orographic factors probably play a role in distinguishing the clouds over the Himalayas and the Rockies; upslope wind flows can have substantial effects on vertical velocity fields. The Himalayas show activity in the band-pass high cloudiness, but not in the band-pass-filtered 500-mb streamfunction; Fig. 1 of WLB shows considerable activity in the filtered 1000-mb streamfunction in this region.

The relative maximum in band-pass streamfunction standard deviation over the Mediterranean (Fig. 1b) is not found in the corresponding plot for high cloudiness (Fig. 1d). A relative maximum in the standard deviation of band-pass mid-level cloudiness is obtained over the Mediterranean instead (not shown).

## 4. Spatial correlations of height and cloud area

Spatial correlations have been used to describe variations in the observed fields of OLR (Cahalan et al. 1982) and geopotential height (i.e., Wallace and Gutzler 1981) and to validate GCM radiation simulations with satellite data (Charlock et al. 1988). Here spatial correlations were used to establish the climatological phase relationships between the fields of geopotential height and high cloudiness in the baroclinic waveguides. All of the data used in this section have been band-pass filtered. The focus will be on two regions in the Atlantic and Pacific waveguides that have substantial correlations between cloudiness and geopotential height. The Atlantic region that has been selected provides an example of the relationship between geopotential height and high cloudiness near the center of a

midlatitude baroclinic waveguide (the center is defined by the standard deviation maximum of the band-pass geopotential streamfunction in Fig. 1b). The Pacific region that has been selected provides an example of this relationship near the entrance of a waveguide. A general view of the relationship between geopotential height and high cloudiness over the northern extratropics will be given in section 5.

Figure 2a displays the spatial correlation of the 500-mb height base grid point at 40°N, 70°W (identified by an asterisk) with other 500-mb heights for the six-winter record. Blackmon et al. (1984a) present and discuss this field for a different temporal record. Centers of negative correlation are located to the east and west of the base grid point. The centers of negative correlation denote positions approximately one-half wavelength from the base grid point. A climatological wavelength of 50° of longitude (about 4300 km) is observed for the geopotential height in Fig. 2a.

In Fig. 2b the 500-mb height at the same base grid point (40°N, 70°W) has been correlated with the full spatial field of the high cloudiness. It must be stressed that Fig. 2b is a height–cloud correlation, while Fig. 2a is a height–height correlation. The magnitudes of the correlations in Fig. 2b have been considerably diminished from those in Fig. 2a. A SW–NE spatial orientation is noted in both the 500-mb (Fig. 2a) and high cloud (Fig. 2b) correlates of the 500-mb height.

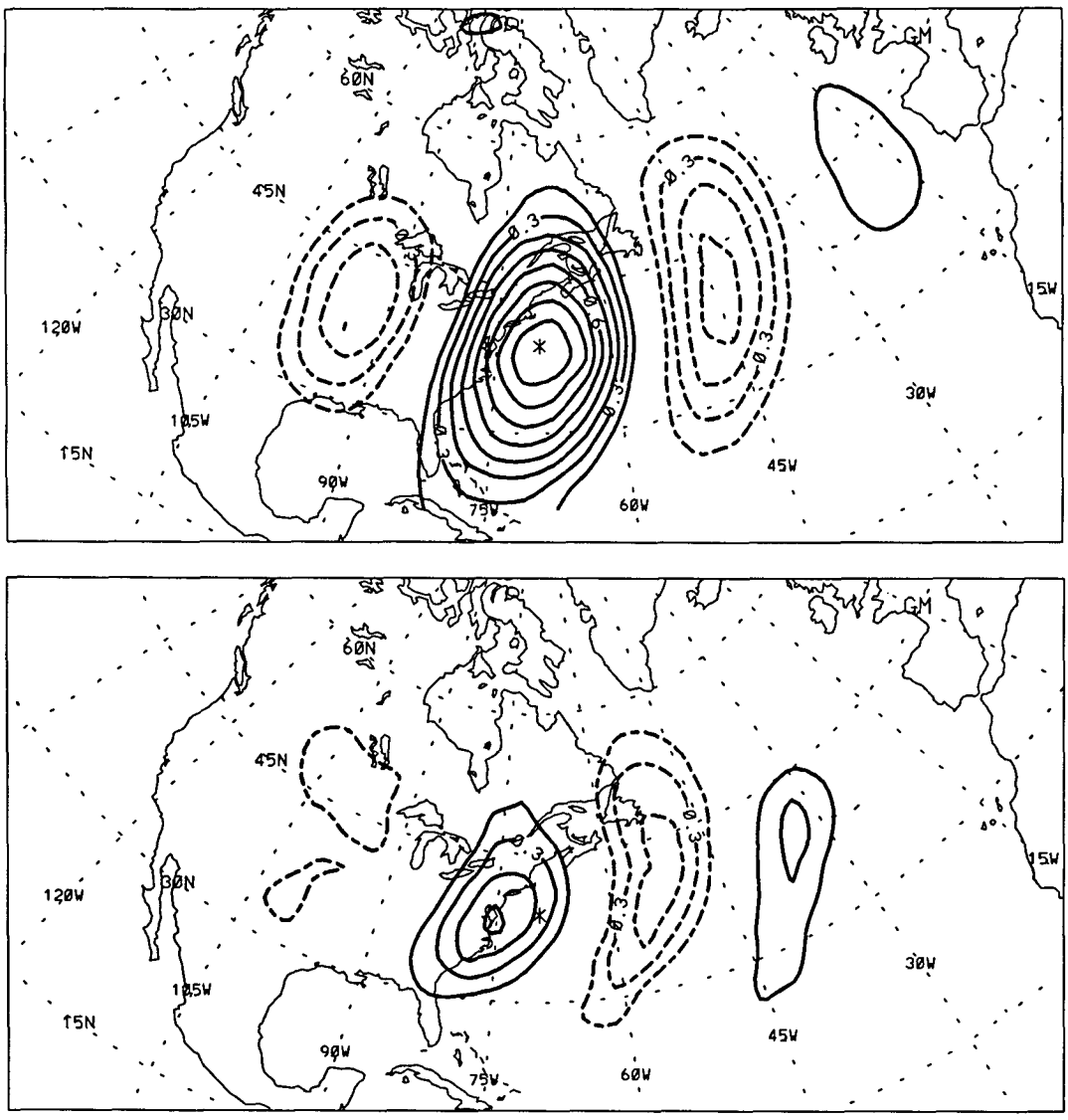


FIG. 2 (a) Band-pass correlation of the 500-mb height at the base grid point (marked by an asterisk) with the 500-mb height at all other points. Contours plotted have an absolute value of 0.2 or greater; contour interval 0.1. Negative contours are dashed. (b) Band-pass correlation of the 500-mb height at the base grid point (marked by an asterisk) with the high cloud area at all other points. Contours as in (a).

In Fig. 2b a negative correlation with the high-cloud field is found roughly 18° of longitude to the east from the 500-mb base grid point; a positive correlation is found 7° to the west. There is an east–west asymmetry in the displacements of the negative (18°) and positive (7°) signals from the base grid point in the height–cloud correlation (Fig. 2b). In a quasi-geostrophic system (Holton 1979), the height and the vertical velocity are symmetrically displaced and separated in phase by one-fourth of a wavelength. An asymmetrical displacement of about one-third of a wavelength was found for the negative height–cloud correlation and about one-sixth of a wavelength for the positive height–cloud correlation as given in Fig. 2b.

Figure 2b was developed from a six-winter record of Nimbus-7 and NMC data. Because Nimbus-7 data and NMC data are generally asynoptic, the analysis of Fig. 2b was repeated with ISCCP data as a test. ISCCP data are available at the 0000 UTC and 1200 UTC NMC observing times. The ISCCP cloud retrievals were available for one three-month winter (December 1983–February 1984), for which the analysis with the Nimbus-7 retrievals was also repeated. For this short length of record, both the ISCCP and Nimbus-7 plots (not shown) displayed a considerable amount of noise, especially at large distances from the base grid point. The magnitudes, shapes, locations, and orientations of the height–cloud correlations near the 500-mb base grid point correspond very closely for the ISCCP and Nimbus-7 data.

Are the high-cloud correlations of Fig. 2b associated primarily with negative (trough) or positive (ridge) excursions of the 500-mb height at the base grid point? This was answered by identifying all points in the 500-mb height time series at the base grid point that are respectively greater than one standard deviation above or less than one standard deviation below the mean; composites were then formed of the high-cloud field (in standard deviation units of high cloudiness) corresponding to the positive (Fig. 3a) and negative (Fig. 3b) deviations in 500-mb height at the base grid point. The height–cloud correlation of Fig. 2b appears to be associated uniformly with both positive and negative excursions of the height at the base grid point. Height anomalies at the base grid point of one standard deviation unit or larger are associated with spatially displaced high-cloud anomalies as large as 0.7 standard deviation units (Figs. 3a and 3b).

Fig. 4a displays the spatial correlation of a 500-mb height base grid point in the Pacific Ocean with other 500-mb heights. For the Pacific height–cloud correlation (Fig. 4b), note that the eastward displacement (from the base grid point) of the area of strongest negative correlation is longer than the westward displacement (from the base grid point) of the area with the strongest positive correlation; this was also found for the Atlantic height–cloud correlation (Fig. 2b). However, the Pacific height–cloud correlation is more circular (Fig. 4b) than is the elongated Atlantic pattern (Fig. 2b). The base grid point in Figs. 4a,b is located in the western sector of a baroclinic waveguide, while the base grid point of Figs. 2a,b is located near the center of a waveguide (Fig. 1b). Height–cloud correlations tend to be elongated N–S when the base grid points are near the center or in the eastern sectors of the waveguides.

To further investigate the spatial structures of the geopotential and cloud fields, height–height correlations (i.e., Figs. 2a and 4a) and cloud–cloud correlations have been compared. Cloud–cloud correlations are developed by correlating the high-cloud field at a base grid point with the high-cloud field at all other grid points. The strongest negative values in height–height correlations are typically −0.6 in the baroclinic waveguides (see also Fig. 16 in Blackmon et al. 1984a). In the same regions, the strongest negative values in the cloud–cloud correlations (not shown) are commonly −0.3 to −0.4. As the absolute magnitudes of the strongest negative correlations for high clouds (0.3) are less than those for heights (0.6), it is suggested that high-cloud fields are less wavelike than height fields in the band-pass regime.

Time-lagged correlations of the OLR (Cahalan et al. 1982) have been used to investigate the movement of OLR fluctuations. The movements of height fluctuations have also been studied with time-lagged correlations (Blackmon et al. 1984b, Fig. 1) A comparison of time-lagged height–height, height–cloud, and cloud–cloud correlations indicates that the band-pass high-cloud fluctuations tend to move with the 500-mb height fluctuations (not shown).

## 5. Summary of extratropical height–cloud correlations

### *a. Summary maps defined*

WLB used the term *teleconnectivity* to describe the extent to which geopotential height fluctuations are wavelike. They defined the teleconnectivity of a grid point as "the absolute value of the strongest negative correlation appearing on the one-point correlation map for that grid point." Teleconnectivity plots can be used to characterize the approximate wavelengths and orientations of the height fluctuations. While the term *teleconnection* (i.e., Wallace and Gutzler 1981) is often associated with very large-scale low-frequency processes, teleconnectivity plots have been found to be useful for analyzing processes at various scales. WLB used teleconnectivity plots to demonstrate that height fluctuations are wavelike in regions that exhibit high standard deviations in the high-pass-filtered geopotential streamfunction field (the baroclinic waveguides). The teleconnectivity in the band-pass-filtered 500-mb geopotential streamfunction (not shown) was computed and found that it corresponded very well with the high-pass-filtered teleconnectivity field in Fig. 6 of WLB.

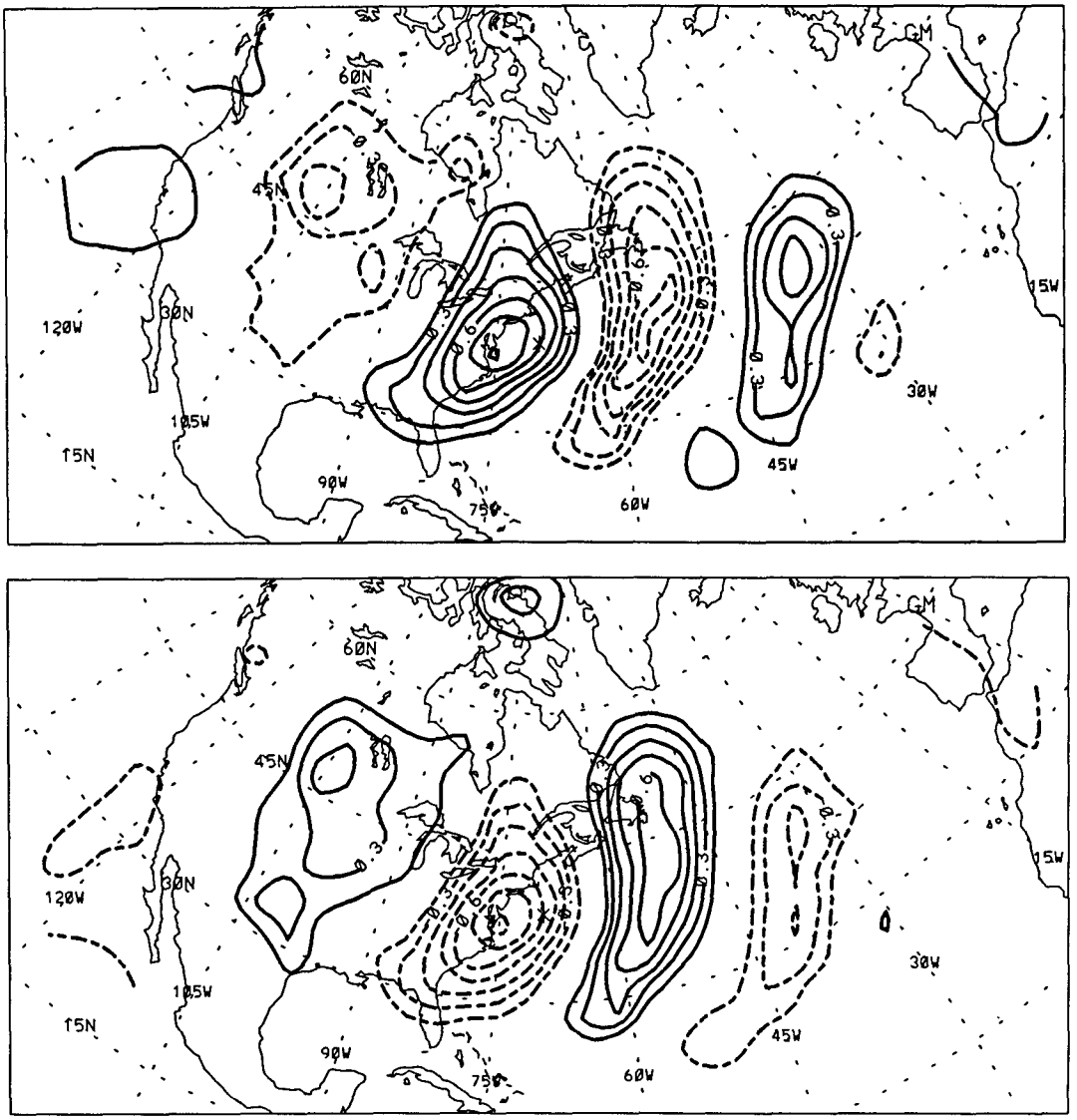


FIG. 3. (a) Composite of band-pass high cloudiness expressed in fractional units of standard deviation of the high cloudiness at each grid point from its long-term mean. Composite formed from the points in the time series for which the band-pass 500-mb height at the base grid point (marked with an asterisk) is at least one standard deviation above its mean. Contours as in Fig. 2a. (b) As in (a), but formed from the points in the time series for which the 500-mb height at the base grid point is at least one standard deviation below its mean.

The correlation between the band-pass-filtered 500-mb height time series at each grid point and the high cloudiness at the grid point with which it exhibits the strongest positive (Fig. 5a) and negative (Fig. 5b) correlation was then plotted. Figures 5a,b were constructed by 1) correlating the 500-mb time series at each base grid point with the cloud time series at all extratropical grid points and 2) assigning to each 500-mb base grid point the value and location of the strongest positive (Fig. 5a) or negative (Fig. 5b) correlation with the high clouds. Arrows are directed from the 500-mb base grid points toward the centers of the strongest positive (Fig. 5a) or negative (Fig. 5b) correlations with the high clouds. Each arrow extends 30 percent of the distance from the 500-mb base grid point to the geographical point with which it exhibits the strongest positive (Fig. 5a) or negative (Fig. 5b) correlation in the high-cloud time series.

Figures 5a,b can be considered as generalizations of Figs. 2b and 4b. In Fig. 2b, for example, the strongest positive correlation of the height with the cloudiness is found to the west of the base grid point (marked by an asterisk). Note the arrow, drawn to 30 percent scale, is at this grid point in Fig. 5a. If the arrow had been

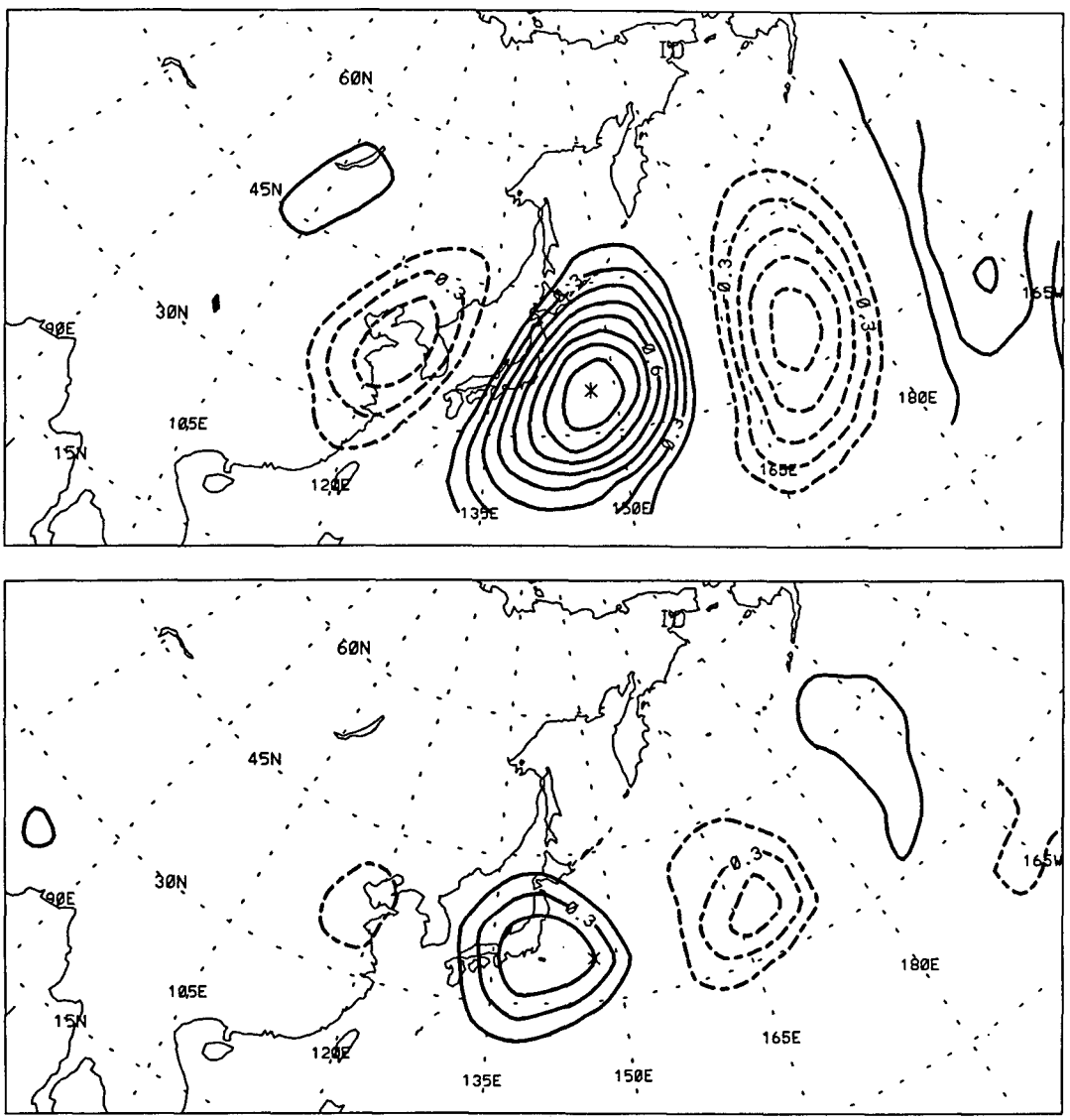


FIG. 4 (a) As Fig. 2a, but for a base grid point in the Pacific. (b) As Fig. 2b, but for a base grid point in the Pacific.

drawn to full scale, it would extend to the point in Fig. 5a that corresponds to the center of the strongest positive correlation seen in Fig. 2b.

*b. Results from summary maps*

The contours in Figs. 5a,b map the values of the strongest positive (Fig. 5a) and negative (Fig. 5b) height–cloud correlations that were determined for each base grid point. The absolute magnitudes of the contours in the vicinity of the baroclinic waveguides at 40°N over the western Atlantic and central Pacific indicate that the height–cloud correlations in those regions are relative geographical extrema. This suggests that the relationships between band-pass fluctuations in high cloudiness and geopotential are most coherent in the waveguides.

In the baroclinic waveguides over both the Atlantic and the Pacific, the strongest positive height–cloud correlations are indicated by the arrows (Fig. 5a) to be due west of the 500-mb height base grid points in many cases. The short arrows in these locations indicate that the strongest positive height–cloud correlations are relatively close to the base grid points; the strongest positive height–cloud correlations are approximately one-sixth of a wavelength in geopotential height to the west of the base grid points. Over the western basins of the Atlantic and Pacific oceans and over eastern North America, the arrows representing the strongest negative height–cloud correlations (Fig. 5b) are longer and di-

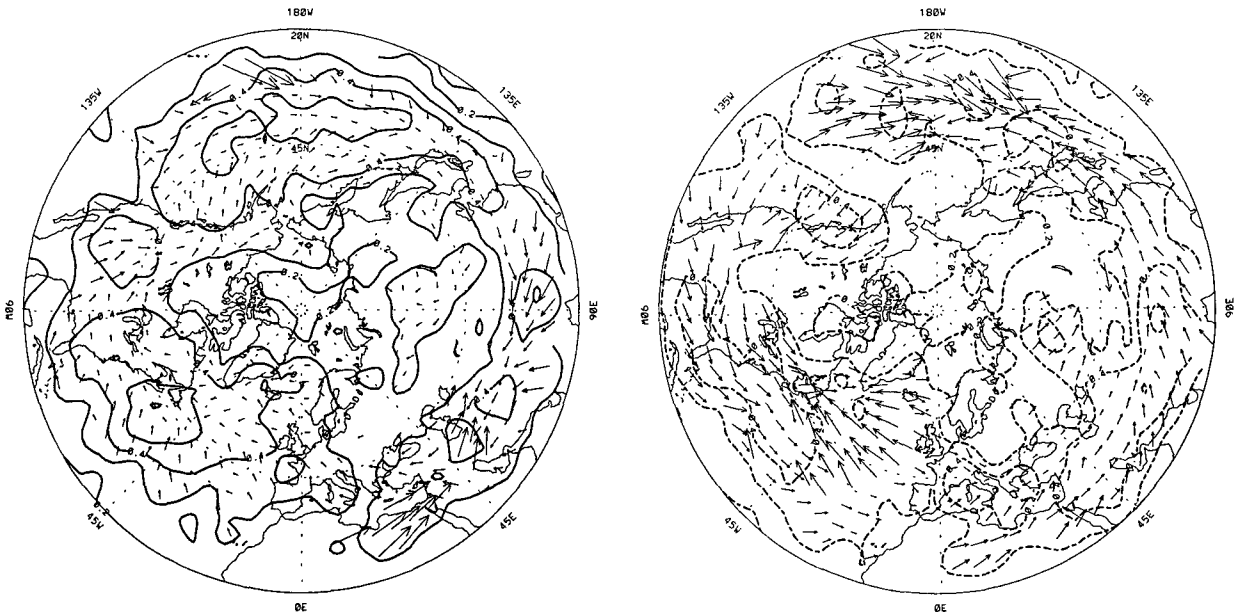


FIG. 5. (a) Correlation between the band-pass-filtered 500-mb height time series at each grid point and the band-pass high-cloud area at the grid point with which it shows the strongest positive correlation. Contours as in Fig. 2a. The arrows are directed toward the grid point with the cloudiness that is most strongly positively correlated with the 500-mb height at the base grid point. The length of the arrow is drawn at 30 percent scale. Arrows are not drawn for grid points having a correlation with an absolute value below 0.3. (b) As in (a), but the correlation that shows the strongest negative value is plotted. The arrows are also directed toward the grid point with the cloudiness that is most strongly negatively correlated with the 500-mb height at the base grid point.

rected toward the east from the same base grid points; these longer arrows indicate that the strongest negative height–cloud correlations are approximately one-third of a wavelength in geopotential height to the east of the base grid points.

The arrows in Figs. 5a,b are consistent with the following simple description of the spatial phase relationships between high clouds and 500-mb heights in the baroclinic waveguides: positive anaomalies in high cloudiness tend to be located one-third of a wavelength to the east of troughs, and negative anomalies in high cloudiness tend to be located one-sixth of a wavelength to the west of troughs. The height–cloud spatial phase relationships denoted by the lengths and directions of the arrows representing the strongest positive correlations (Fig. 5a) are nearly constant over the Pacific between 35°N and 40°N; a similar constancy is found over the Atlantic at 50°N.

Figure 5b shows that while the arrows representing the strongest negative correlations between height and cloudiness are generally directed toward the east from the 500-mb base grid points, there are two large areas with arrows that are directed toward the west. Arrows in Fig. 5b are directed toward the west over the centers of the Atlantic (45°W) and Pacific (175°W) oceans. Strong baroclinic wave activity is located to the west of these regions, and the strongest negative height–cloud correlations are generally to the west of the base grid points, toward the center of the waveguide. A similar effect is seen over the subtropics in both the positive (Fig. 5a) and negative (Fig. 5b) height–cloud correlation fields; the subtropical arrows often point north, toward the midlatitude waveguides. WLB in his Fig. 6 described such features in the geopotential height teleconnectivity fields.

Over much of southern Asia at 30°N, we have positive arrows (Fig. 5a) directed westward from the base 500-mb height grid points and negative arrows (Fig. 5b) directed eastward. Two cases that relate to the arrows representing the strongest positive height–cloud correlations (Fig. 5a) over Asia are regarded as noteworthy. First, in some locations such as Tibet (30°N, 90°E), the lengths of the positive arrows (Fig. 5a) exceed the lengths of the negative arrows (Fig. 5b). Second, in other areas (near the Zagros Mountains at 30°N, 50°E) the positive arrows (Fig. 5a) are reversed and directed eastward. The relationships between the positive (Fig. 5a) and negative (Fig. 5b) arrows in these two cases over Asia are different than the relationships found over the oceanic baroclinic waveguides. In both cases over Asia, the phase relationships between clouds and 500-mb heights that were found in the oceanic waveguides may be obscured by the effects of mountains that induce the formation of orographic waves. During the NH winter, a zonally oriented subtropical 500-mb jet is located over northern Africa and southern Asia at about 25°N (see Fig. 6a in Blackmon et al. 1977). Terrain influences on this jet can result in oro-

graphic waves with phase relationships between the geopotential, cloud, and vertical velocity fields that are quite different from the phase relationships found with oceanic baroclinic waves.

Over the Rocky Mountains, base grid points at 500-mb have their strongest positive correlations with high clouds well to the northwest (Fig. 5a). WLB noted in their Fig. 7 a pronounced SE–NW tilt in the correlations between the 1000-mb and 500-mb height fields over the Rockies.

## 6. Discussion

Over many regions in the baroclinic waveguides, a general east–west asymmetry was found in the band-pass correlation of the full field of high cloudiness with specified base grid points in the 500-mb height: a positive deviation in high cloudiness is roughly one-third of a wavelength to the east of the axis of a trough in band-pass 500-mb height, and a negative deviation in high cloudiness is roughly one-sixth of a wavelength to the west of the trough. These results are consistent with the jet stream study of Durran and Weber (1988), which focused on three synoptic cases. Synopticians draw a similar picture: high-cloud fields overrun well ahead of midlatitude troughs, and rapid clearing is obtained close behind them.

This paper is focused on band-pass (2.5–6.0 day) processes. In much lower frequency processes, increases in high cloudiness are also observed to the east of midlatitude oceanic troughs (Liebmann and Hartmann 1984; Charlock et al. 1990).

The analysis in section 3 suggested that short-period baroclinic wave activity, rather than the seasonal mean vertical velocity field forced mostly by the time-mean circulation, generates the seasonal mean midlatitude maxima in high-cloud areas over the Atlantic and Pacific oceans. The relationship between the band-pass fields of high cloudiness and vertical velocity can also be tenuous. In a given synoptic system (i.e., Durran and Weber 1988), clouds can be expected to respond to fluctuations not only in vertical velocity, but also to fluctuations in other fields such as water vapor and radiation. Great care must be taken in interpreting a large-scale phase relationship between height and cloudiness as a possible signal of a phase relationship between height and vertical velocity. It is likely that many high clouds form over the regions with strong upward vertical velocity, and that they are subsequently advected to the east of the vertical velocity maximum before dissipating. It should be noted, however, that some dynamical models generate positive vertical velocity fields slightly more than one-fourth of a wavelength to the east of midlatitude geopotential troughs, where many high cloud fields were found in this study. Gall (1976, Fig. 16) shows such a phase relationship between vertical velocity and geopotential height for both a linear primitive equation model and a spectral GCM.

Geopotential heights at different levels have been used by various researchers to investigate the vertical structures of tropospheric disturbances (i.e., Blackmon et al. 1979; WLB; Hsu and Wallace 1985; Dole 1986). The correlation of the 500-mb height at a fixed point with the 1000-mb height at the same point is generally positive; the large changes in this fixed-point correlation found by Blackmon et al. (1979) in different time bands strongly suggest that the fixed-point correlation is not simply dominated by the height analysis assumptions over most locations. Here it is noted that the correlations (not fixed-point) between the 500-mb height and high cloudiness (Figs. 5a and 5b) are weaker than the comparable correlations between the 500-mb height and the 1000-mb height (Fig. 7 in WLB). The present results thus suggest that the high-cloud structures of baroclinic waves are less spatially coherent than the internal geopotential-height structures. The high-cloud structures are most coherent in the baroclinic waveguides. The waveguides contain large amounts of high cloudiness.

In section 4 it was noted that the absolute magnitudes of the strongest negative height–height correlations (Figs. 2a and 4a) are generally larger than the absolute magnitudes of the strongest negative cloud–cloud correlations. It appears that band-pass fluctuations in geopotential are more wavelike than band-pass fluctuations in high cloudiness.

Ramanathan et al. (1983) have shown that the infrared radiation associated with high clouds can have a systematic impact on the seasonal mean circulation in a GCM. Cloud radiation can perturb the atmospheric temperature profile at a rate of a few degrees Kelvin per day and thereby affect the transient, as well as the mean, circulation. Radiative transfer calculations indicate that high clouds induce infrared cooling aloft in midlatitudes during winter, and high clouds have a tendency (Figs. 5a,b) to be situated in the warm sectors (Hartmann 1974, Fig. 13) of 500-mb baroclinic waves. Do the radiative effects of clouds dampen the temperature structures of baroclinic waves? The answer to this question depends not only on the high clouds, but also on the low and middle clouds, which are much more difficult to retrieve accurately with satellite data. An assessment of the phase relationships of low and middle clouds to geopotential, and the appropriate radiative budget calculations, is beyond the scope of this paper. The conclusions are confined to the effects of high clouds.

If the high clouds exert a significant radiative impact on the transient baroclinic waves, the generally small value of the height–cloud correlation found here would suggest that the radiative impact on the waves themselves would vary considerably between individual waves. As the height–cloud correlation is strongest

within the baroclinic waveguides, it is within the waveguides where one would expect to find the most systematic high-cloud radiative effects on transient disturbances.

*Acknowledgments.* We thank Roy Jenne and Dennis Joseph at NCAR for assistance in procuring the 500-mb data. A presentation by Larry L. Stowe prompted us to use the Nimbus-7 THIR/TOMS cloud retrievals. G. Louis Smith provided encouragement and critical comments during the course of this work. William B. Rossow gave useful advice relating to the ISCCP data. Drafts of this paper were kindly reviewed by L. L. Stowe, G. L. Smith, J. Timothy Suttles, and R. Green.

## REFERENCES

Blackmon, M. L., 1976: A climatological spectral study of the 500-mb geopotential height of the Northern Hemisphere. *J. Atmos. Sci.*, **33,** 1607–1623.

——, M. L., J. M. Wallace, N.-C. Lau and S. L. Mullen, 1977: An observational study of the Northern Hemisphere wintertime circulation. *J. Atmos. Sci.*, **34,** 1040–1053.

——, R. A. Madden, J. M. Wallace and D. S. Gutzler, 1979: Geographical variations in the vertical structure of geopotential height fluctuations. *J. Atmos. Sci.*, **36,** 2450–2466.

——, Y.-H. Lee and J. M. Wallace, 1984a: Horizontal structure of 500-mb height fluctuations with long, intermediate, and short time scales. *J. Atmos. Sci.*, **41,** 961–979.

——, ——, —— and H.-H. Hsu, 1984b: Time variation of 500-mb height fluctuations with long, intermeditate, and short time scales as deduced from lag-correlation statistics. *J. Atmos. Sci.*, **41,** 981–991.

Cahalan, R. F., D. A. Short and G. North, 1982: Cloud fluctuation statistics. *Mon. Wea. Rev.*, **110,** 26–43.

Charlock, T. P., K. M. Cattany-Carnes and F. G. Rose, 1988: Fluctuation statistics of outgoing longwave radiation in a general circulation model and in satellite data. *Mon. Wea. Rev.*, **116,** 1540–1554.

——, F. G. Rose and K. M. Cattany-Carnes, 1989: Cross correlations between the radiation and atmospheric variables in a general circulation model and in satellite data. *Mon. Wea. Rev.*, **117,** 212–220.

——, ——, T. D. Bess and G. L. Smith, 1990: The relationship of extratropical outgoing longwave radiation to monthly geopotential teleconnection patterns. *J. Climate*, **3,** 1390–1399.

Dole, R. M., 1986: Persistent anomalies of the extratropical Northern Hemisphere wintertime circulation: structure. *Mon. Wea. Rev.*, **114,** 178–207.

Durran, D. R., and D. B. Weber, 1988: An investigation of the poleward edges of cirrus clouds associated with midlatitude jet streams. *Mon. Wea. Rev.*, **116,** 702–714.

Gall, R., 1976: A comparison of linear baroclinic instability theory with the eddy statistics of a general circulation model. *J. Atmos. Sci.*, **33,** 349–373.

Gutzler, D. S., and K. C. Mo, 1983: Autocorrelation of Northern Hemisphere geopotential heights. *Mon. Wea. Rev.*, **111,** 155–164.

Hartmann, D. L., 1974: Time spectral analysis of midlatitude disturbances. *Mon. Wea. Rev.*, **102,** 319–328.

Holton, J. R., 1979: *An Introduction to Dynamic Meteorology.* 2nd ed. Academic Press, 391 pp.

Hsu, H.-H., and J. M. Wallace, 1985: Vertical structure of wintertime teleconnection patterns. *J. Atmos. Sci.*, **42,** 1693–1710.

Kuo, H.-L., 1953: Three-dimensional disturbances in a baroclinic zonal current. *J. Meteor.*, **9,** 260–278.

Liebmann, B., and D. L. Hartmann, 1984: An observational study of tropical–midlatitude interaction on intraseasonal time scales during winter. *J. Atmos. Sci.*, **41,** 3333–3350.

Ramanathan, V., E. R. Pitcher, R. C. Malone and M. L. Blackmon, 1983: The response of a general circulation model to refinements in radiative processes. *J. Atmos. Sci.*, **40,** 605–630.

Rossow, W. B., L. C. Garder and P.-J. Lu, 1988: International Satellite Cloud Climatology Project (ISCCP) documentation of cloud data. World Climate Research Programme, 78 pp. [Available from NASA GISS, 2880 Broadway, New York, NY 10025.]

Schiffer, R. A., and W. B. Rossow, 1985: ISCCP global radiance dataset: a new resource for cloud research. *Bull. Amer. Meteor. Soc.*, **66,** 1498–1505.

Stowe, L. L., C. G. Wellemeyer, T. F. Eck, H.-Y. M. Yeh and the Nimbus-7 Cloud Data Processing Team, 1988: Nimbus-7 global cloud climatology. Part I: Algorithms and validation. *J. Climate*, **1,** 445–470.

——, H. Y. M. Yeh, T. F. Eck, C. G. Wellemeyer, H. L. Kyle and the Nimbus-7 Cloud Data Processing Team, 1989: Nimbus-7 global cloud climatology. Part II: First year results. *J. Climate*, **2,** 671–709.

Trenberth, K. E., and J. G. Olson, 1988: Evaluation of NMC global analyses: 1979–1987. NCAR Tech. Note 299+STR, 82 pp. [Available from NCAR, P.O. Box 3000, Boulder, CO 80307.]

Wallace, J. M., and D. S. Gutzler, 1981: Teleconnections in the geopotential height field during the Northern Hemisphere winter. *Mon. Wea. Rev.*, **109,** 784–812.

——, G.-H. Lim and M. L. Blackmon, 1988: Relationship between cyclone tracks, anticyclone tracks, and baroclinic waveguides. *J. Atmos. Sci.*, **45,** 439–462.

White. G. H., 1983: Estimates of the seasonal mean vertical velocity fields of the extratropical Northern Hemisphere. *Mon. Wea. Rev.*, **111,** 1418–1433.